Correspondence to:

D. R. Weimer,
dweimer@vt.edu

Comparison of a Neutral Density Model With the SET HASDM Density Database

Daniel R. Weimer[1,2] , **W. Kent Tobiska[3]** , **Piyush M. Mehta[4]** , **R. J. Licata[4]** , **Douglas P. Drob[5]** , and **Jean Yoshii[3]**

[1]Center for Space Science and Engineering Research, Virginia Tech, Blacksburg, VA, USA, [2]National Institute of Aerospace, Hampton, VA, USA, [3]Space Environment Technologies, Los Angeles, CA, USA, [4]Department of Mechanical and Aerospace Engineering, Statler College of Engineering and Mineral Resources, West Virginia University, Morgantown, WV, USA, [5]Space Science Division, U.S. Naval Research Laboratory, Washington, DC, USA

Abstract The EXospheric TEMperatures on a PoLyhedrAl gRid (EXTEMPLAR) method predicts the neutral densities in the thermosphere. The performance of this model has been evaluated through a comparison with the Air Force High Accuracy Satellite Drag Model (HASDM). The Space Environment Technologies (SET) HASDM database that was used for this test spans the 20 years 2000 through 2019, containing densities at 3 hr time intervals at 25 km altitude steps, and a spatial resolution of 10° latitude by 15° longitude. The upgraded EXTEMPLAR that was tested uses the newer Naval Research Laboratory MSIS 2.0 model to convert global exospheric temperature values to neutral density as a function of altitude. The revision also incorporated time delays that varied as a function of location, between the total Poynting flux in the polar regions and the exospheric temperature response. The density values from both models were integrated on spherical shells at altitudes ranging from 200 to 800 km. These sums were compared as a function of time. The results show an excellent agreement at temporal scales ranging from hours to years. The EXTEMPLAR model performs best at altitudes of 400 km and above, where geomagnetic storms produce the largest relative changes in neutral density. In addition to providing an effective method to compare models that have very different spatial resolutions, the use of density totals at various altitudes presents a useful illustration of how the thermosphere behaves at different altitudes, on time scales ranging from hours to complete solar cycles.

Plain Language Summary A recently developed computer model predicts the mass density of atoms and molecules in upper atmosphere, in the region known as the thermosphere. Changes in this "neutral density" following geomagnetic storms can perturb the orbits of the many satellites in this region, leading to imprecise knowledge of their paths and risk of collisions. This model uses measurements of the solar wind and the embedded magnetic field to predict the level of heating in the upper atmosphere, and the resulting expansion of the atmosphere to higher altitudes. In order to test the capabilities of the new model, its calculations were compared with density values derived by an Air Force data assimilation system based on radar tracking of multiple objects in Earth orbit over a 20-year period. The results of this comparison show an excellent agreement, particularly at the higher altitudes where geomagnetic storms have the greatest influence.

1. Introduction

A major focus of space weather research has been on the topic of the mass density of the neutral atoms and molecules in the thermosphere. As the variations in this density perturb the orbital motion of satellites, there has been considerable effort in being able to predict these variations using both empirical models and numerical simulations (Bruinsma et al., 2018; Emmert, 2015).

Recently Weimer et al. (2020) had described a new empirical model that calculated exospheric temperatures, the asymptotic limit that the temperature in the thermosphere reaches at high altitudes (Prölss & Bird, 2004), often abbreviated as either T_{ex} or T_{∞}. The temperature inputs to the model were derived from neutral density measurements from multiple satellites. Data from the Challenging Mini-satellite Payload (CHAMP) (Bruinsma et al., 2004; Reigber et al., 2002) in the years 2002 through 2009 were used, along with the Gravity Recovery and Climate Experiment (GRACE) satellites (Tapley et al., 2004), from 2003 through 2010. These total mass densities were derived from accelerometer measurements of the orbital drag. In our work we use density data from the CHAMP and GRACE missions provided by Mehta et al. (2017), who had recalibrated the drag coefficients

Visualization: Daniel R. Weimer
Writing – original draft: Daniel R. Weimer
Writing – review & editing: W. Kent Tobiska, Piyush M. Mehta, R. J. Licata, Douglas P. Drob

and provided updated values of the neutral densities. The original data were from Sutton (2008). Additional density data were from the European Space Agency's Swarm mission (Friis-Christensen et al., 2006), for the time period from 30 November 2013 through 2017. Orbital motions obtained from Global Positioning System (GPS) receivers on these spacecraft were used to determine the drag (Astafyeva et al., 2017; van den IJssel et al., 2020).

To create the empirical model, the temperature values were sorted into 1,620 cells on a geodesic, polyhedral grid. These triangular grid cells have nearly equal areas and their edges have arc lengths of approximately 7°. Multiple linear regression fits were then used to obtain an equation for the exospheric temperature at each cell's specific location, as a function of the input parameters. For convenience, the unique acronym EXTEMPLAR was given to this method, for EXospheric TEMperatures on a PoLyhedrAl gRid. The Naval Research Laboratory Mass Spectrometer and Incoherent Scatter radar Extended (NRLMSISE-00) thermosphere model (Hedin, 1991; Picone et al., 2002) was originally used to convert the density measurements into the exospheric temperatures values that were used for the model development (For this paper we use the newer, NRLMSIS 2.0 model [Emmert et al., 2020]). Afterward the "MSIS" model (as commonly known) was used to calculate neutral densities using the exospheric temperatures output from EXTEMPLAR for given locations and input parameters. Comparing such density predictions with the original satellite measurements revealed a very good performance by the combination of the EXTEMPLAR and MSIS models (hereafter referred to as simply EXTEMPLAR, with the MSIS component assumed). As there were on the order of ≈100,000 data points in each grid cell, the regression formulas that used only six input variable and 16 coefficients could not contain a memory of specific time periods or events, so this was considered a valid test of the model. Nevertheless, a validation trial using an independent data set is valuable.

The Air Force High Accuracy Satellite Drag Model (HASDM) (Storz et al., 2005) assimilates radar tracking of several dozens of calibration satellites to obtain thermospheric neutral densities. HASDM continuously adjusts coefficients in a modified Jacchia-Bowman 2008 (JB2008) model (Bowman et al., 2008; Tobiska et al., 2008) to match the radar measurements. While the Combined Space Operations Center (CSpOC) of the United States Space Force (USSF) (previously part the Air Force) archives the temperature-correction coefficients that have been applied to the JB2008 atmosphere, these data are not available to the public. Space Environment Technologies (SET) validates the HASDM outputs under contract and produces a recreation of the densities of the global atmosphere, calling it the "SET HASDM density database" (Tobiska et al., 2021). With approval of the USSF, SET has released the density values for scientific use. These data span two solar cycles, from 1 January 2000 through 31 December 2019. As stated by Tobiska et al. (2021), "all solar cycle, geomagnetic storm and substorm, extended solar flare, and thermospheric cooling perturbations are embedded in the data. Because of its accuracy, time resolution, global scale, and information content, the SET HASDM database densities are suitable for use as a new space weather benchmark for atmospheric expansion against which space weather events are measured." The purpose of this paper is to present the results of a comparison between the EXTEMPLAR and HASDM density values. The comparison was run for the entire, 20-year time period with a newer version of the EXTEMPLAR model described in Section 3. In addition to serving as a useful validation tool, the results have provided helpful insights into the behavior of the thermosphere over the two solar cycles.

2. Density Calculations Using NRLMSIS

It is helpful to review how the MSIS model is used with the EXTEMPLAR program in order to obtain the neutral densities. This description helps with understanding some of the results that will be shown. The standard input parameters for MSIS are the geographic coordinates, altitude, date, time, solar $F_{10.7}$ index (both daily and 81-day average), and the daily A_p index of geomagnetic activity. There is an option to include values of the ap index over six, 3-hr intervals. To obtain the neutral densities in the thermosphere, NRLMSIS 2.0 calculates the density of each atomic and molecular species at a boundary at 122.5 km altitude, along with the temperature and temperature gradient. Normally, MSIS also calculates the exospheric temperature for the given conditions and coordinates. The boundary conditions and exospheric temperature are then used to compute the density of each species as a function of altitude, as illustrated in the example in Figure 1. The species densities are summed to obtain the total density (the black line in the figure).

One shortcoming to the MSIS model is that the actual values of the A_p index are obtained only after measurements from magnetometers at selected, global locations are processed. So real-time indices are not available. While
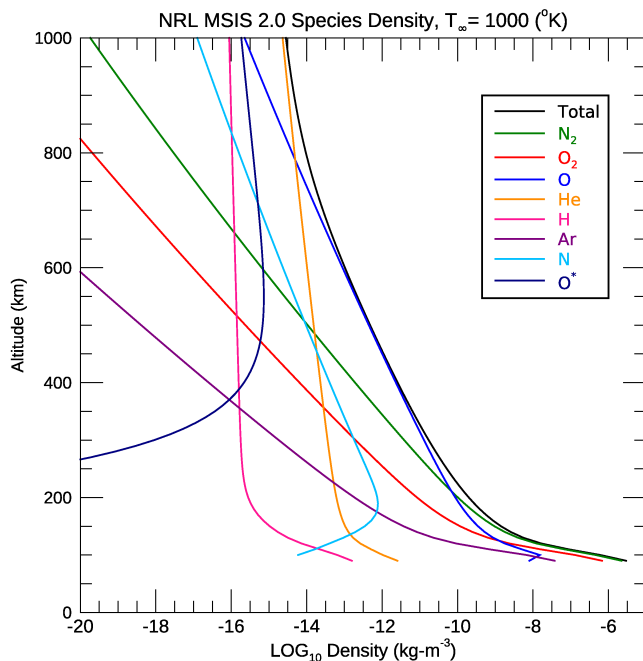
Figure 1. Example of densities from NRLMSIS 2.0 as a function of altitude. All species that are calculated are shown, using colors indicated in the legend. Total density shown in black. Input values were 80° latitude, 0 longitude, on Spring equinox at 0 Universal Time. $F_{10.7}$ index was 120 sfu, and A_p index zero, with exospheric temperature set to 1,000°K.

there are predictions of A_p available, they are only estimates. As geomagnetic indices are only an indirect proxy for the amount of heating that occurs in the polar regions, it is assumed that a model of the Poynting flux should be more accurate, as this energy flux has a more direct, physics-based relationship with the temperature changes. Furthermore, as the solar wind velocity and IMF values are the primary input needed to obtain the Poynting flux, values can be obtained from real-time measurements having an approximately 1 hr lead time, rather than much later. This lead time results from the time it takes the solar wind and IMF to travel from a satellite monitor located at an "upstream" position (Case & Wild, 2012) while the measurement data that are transmitted arrive much sooner. The physical relationship between the energy flux and temperatures plus the lead time are two reasons why the use of exospheric temperatures from the EXTEMPLAR model is advantageous. It also uses the solar indices S_{10} and M_{10}, that are considered to be more accurate than $F_{10.7}$ alone since they represent the actual solar irradiance being deposited into the thermosphere (Bowman et al., 2008; Tobiska et al., 2008).

With a small modification to the MSIS program, the exospheric temperature that is calculated by the EXTEMPLAR model is included as a new input parameter. This temperature (if included in the input parameters) replaces the value that MSIS calculates internally. Figure 2 illustrates the effect of changing the exospheric temperature in MSIS, with densities as a function of altitude shown for temperatures of 600, 1,000, 1,400, 1,800, and 2,200°K. Note that at an altitude of 200 km, the exospheric temperature variations have little effect on the modeled density.

3. Recent EXTEMPLAR Modifications

Work is presently under way to improve the EXTEMPLAR method and develop a real-time, operational program, so the version used in this comparison is similar to but not exactly identical to what was described by Weimer et al. (2020). One difference is that the we now use the newer NRLMSIS 2.0 model (Emmert et al., 2020) rather than NRLMSISE-00. This change will enable use of future updates to this model, but it also resulted in a need to recalculate all temperature values used in the EXTEMPLAR model development, the reason being that the newer version of the MSIS model produces densities lower than the original version for the same input conditions.

An exospheric temperature is derived from a density with use of the MSIS model by means of a reiterative substitution of revised exospheric temperatures in the model until the model's output density at the given coordinates matches the measured value. The bisection method is used, with the search terminating when the resolution is within 2°K. The result is called the measured temperature. The process is repeated for every density measurement in the database.

For this method to work, the density measurements need to match, on average, the unmodified MSIS model as much as possible during or else the derived temperature values may be excessively high or low. The density measurements from the various satellites may need to be multiplied by a correction factor in order to produce the best overall match with the densities from the MSIS model. The process is described by Weimer et al. (2016) using the original CHAMP and GRACE data (Sutton, 2008). Later Weimer et al. (2018) had derived different correction factors for the newer, higher-resolution density values provided by Mehta et al. (2017) for these satellites, and these same factors were used for the original EXTEMPLAR model Weimer et al. (2020). For example, the CHAMP data were all multiplied by a factor of 1.12 before calculating the temperatures. The new NRLMSIS 2.0 model actually matched the CHAMP densities very well without any adjustment, so the correction factor was changed to 1. The correction factor for the GRACE A satellite varies over time from 1. to 1.2, depending on the date, while a factor of 1.08 was used for densities from all Swarm satellites.

The previous work by Weimer et al. (2020) originally had an objective to determine whether or not satellite measurements of emissions from nitric oxide could be used in predictions of thermospheric temperatures and density.
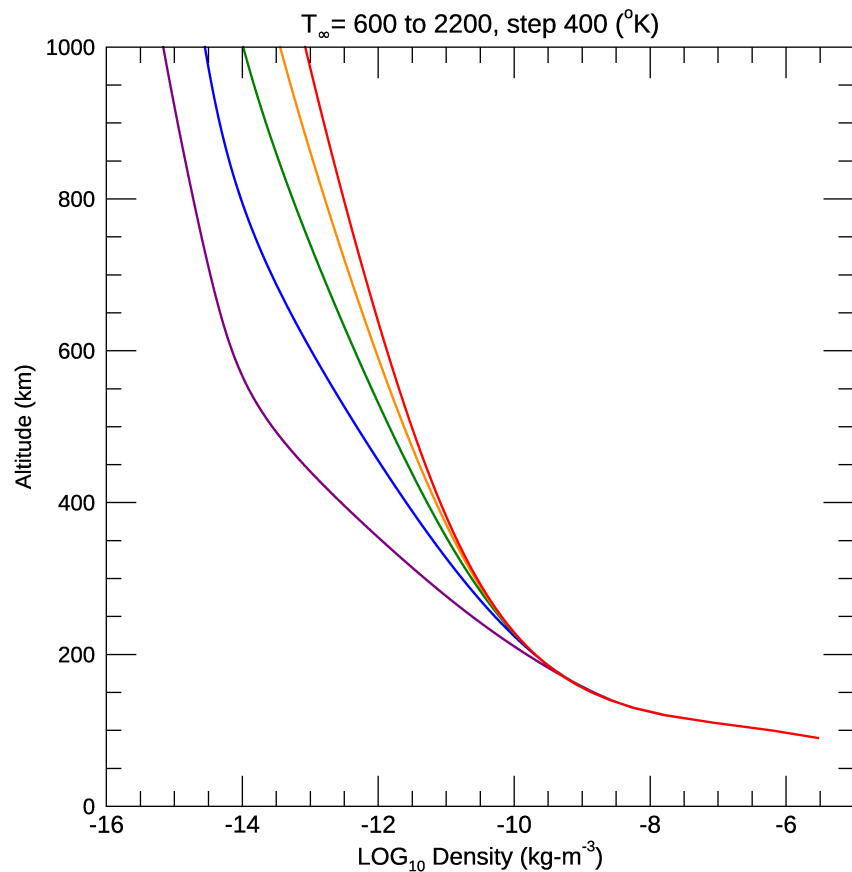
Figure 2. Example of total densities from NRLMSIS 2.0 as a function of altitude, for different values of exospheric temperature. The five lines show results with the exospheric temperature set to 600, 1,000, 1,400, 1,800, and 2,200°K, using the colors purple, blue, green, orange, and red, respectively. Other input parameters are the same as in Figure 1.

Several versions of the EXTEMPLAR formula were reported, with Versions 1 through 5 using the measured nitric oxide emissions in the temperature calculation. The sixth version used a simulated value of the extra cooling due to nitric oxide within a difference equation (details below) rather than measured values. As nitric oxide emission measurements are not presently available in real time, the most recent EXTEMPLAR model is most closely related to the previous Version 6, that used only solar indices and Poynting flux values from an empirical model (Weimer, 2005a, 2005b) that can use historical or real-time solar wind and Interplanetary Magnetic Field (IMF) measurements.

The EXTEMPLAR model that was used in this comparison with the HASDM data is referred to as Version 2.4.2, since is a second-generation model, using the fourth (of several) iterations that were tested, and using version 2 of the NRLMSIS model. As before, the exospheric temperatures are calculated separately for each of 1,620 grid cells; this grid is obtained from a 20-facet icosahedron, in which each facet is subdivided into 81 equilateral triangles, with the new vertices projected outward to a sphere. A new feature is that the Poynting flux values are delayed in time, with different time delays used for each grid cell. The result is that when the auroral heating suddenly increases the temperatures in the grid cells near the pole will increase sooner than at locations near the equator, that have a delayed response. Details about these delays will be reported in a separate publication.

The exospheric temperature in each grid cell is obtained from this formula:

$$
\begin{aligned}
T_{\infty_N} = {} & C_0 + C_1 S_{10} + C_2 S_{10}\sin(\theta_D) + C_3 S_{10}\,\cos(\theta_D) \\
& + C_4\sqrt{M_{10}} + C_5\sqrt{M_{10}}\,\sin(\theta_D) + C_6\sqrt{M_{10}}\,\cos(\theta_D) \\
& + C_7\,\sin(2\theta_D) + C_8\,\cos(2\theta_D) + C_9\,\sin(\phi_{UT}) + C_{10}\,\cos(\phi_{UT}) \\
& + C_{11}S_T(\delta t_N)\sin(\phi_{UT}) + C_{12}S_T(\delta t_N)\cos(\phi_{UT}) + C_{13}S_T(\delta t_N) \\
& + C_{14}\Delta T\sin(\theta_D) + C_{15}\Delta T\cos(\theta_D) + C_{16}\Delta T
\end{aligned}
\tag{1}
$$

T_{∞_N} is the exospheric temperature in cell number N. S_{10}, and M_{10} are solar proxy indices that were developed for use in the JB2008 density model (Thayer et al., 2021; Tobiska et al., 2008). Predictions of these indices are produced by SET, with updated values provided in near real-time. The recent and historical S_{10} and M_{10} solar indices are freely available at the JB2008 website https://spacewx.com/jb2008/while the predicted values are publicly, commercially available through the US Space Force Unified Data Library. θ_D is calculated using $2\pi DOY/365.25$, which is the Day-Of-Year date converted to radians, and $\phi_{UT} = 2\pi UT/24$ is the Universal Time (UT) converted to radians. The C_7 and C_8 terms reproduce semi-annual/inter-annual variations in the data. $S_T(\delta t_N)$ represents Poynting flux values that have been delayed in time by an amount that is unique for each grid cell N. Sums of the Poynting flux are actually calculated for both the Northern and Southern Hemispheres. As described by Weimer et al. (2020), these totals are combined with a formula that varies smoothly from one hemisphere to the other:

$$
S_T = S_N \sin^2(0.5 * (Latitude + \pi/2)) + S_S \sin^2(0.5 * (Latitude - \pi/2))
\tag{2}
$$

where S_N and S_S are the total Poynting flux values in the Northern and Southern hemispheres respectively. The latitude is determined from the coordinates of each grid cell's geometric center. In radians, this latitude ranges from $-\pi/2$ to $+\pi/2$. The Poynting flux values in this version are smoothed with a boxcar averaging function having a width of 1 hr, prior to the application of the time delays, that range from 39 min in polar regions to 6.6 hr at low latitudes.

The ΔT in Equation 1 represent a global perturbation to the exospheric temperature, that varies in each grid cell in proportion to C_{14}, C_{15}, and C_{16}. ΔT varies in time, as calculated with the following numerical difference equation:

$$
\Delta T(t_{n+1}) = \Delta T(t_n) - \Delta T(t_n)\left(\frac{\delta t}{\tau_c}\right) + \alpha S_T(t_n) - P_{NO}(t_n)
\tag{3}
$$

In each time step ΔT increases in proportion (α) to the total Poynting flux in both hemispheres (S_T), and decays at an exponential rate with time constant τ_c. ΔT is further decreased by P_{NO}, which represents the cooling due to nitric oxide emissions. This simulated cooling is calculated with difference equations, using exactly the same methods described by Weimer et al. (2020) in their Equations 10 and 11, rather than using measured emissions. As in the previous versions of the model, the various parameters in the difference equations were optimized through reiterative fits of the T_{∞_N} from Equation 1 with all temperature values in each cell.

4. Comparison With HASDM

The complete SET HASDM density database is available at https://spacewx.com/hasdm/. As indicated by To-biska et al. (2021), this data "covers the period from 1 January 2000 through 31 December 2019. Data records exist every 3 hr during solar cycles 23 and 24. The database has a grid size of $10° \times 15°$ (latitude, longitude) with 25 km altitude steps between 175 and 825 km." One difficulty is that the resolution of this grid is much more coarse than that used in the EXTEMPLAR model, in which the triangular cells have edge lengths of approximately $7°$, and their centers are separated by as little as $4.3°$ between adjacent triangles. As the HASDM model, and the JB2008 model from which it was derived, use spherical harmonics having low order and degree, using smaller grid spacings for the HASDM data archive would not have helped much to improve the resolution of details.
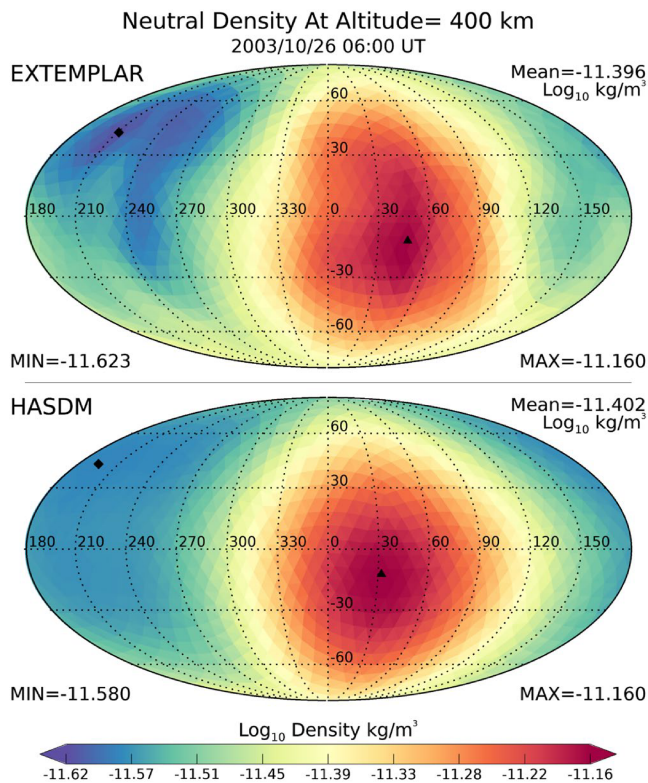
Figure 3. Example of neutral densities from EXTEMPLAR (top) and HASDM (bottom), mapped at 400 km altitude. Values are calculated for 26 October 2003, at 6 hr UT. The values in the upper right corners show the mean values of the densities at this altitude, with minimum and maximum values indicated in the lower left and right corners. All units are the base 10 logarithm of the density in kg/m³.

For purpose of comparison, the HASDM grid values were interpolated to the centers of the geodesic grid cells used in EXTEMPLAR. An example of such a comparison is shown in Figure 3, from 26 October 2003 at 6 hr Universal Time (UT). In this example (and others not shown) it is apparent that the EXTEMPLAR densities have features that do not appear in the HASDM map. On the other hand, comparisons of EXTEMPLAR densities with CHAMP and GRACE measurements had indicated that small-scale variations in the density variations do exist (Weimer et al., 2020). Reports on complex, localized density enhancements had previously been reported on numerous occasions (Bruinsma et al., 2006; Crowley et al., 2010; Schlegel et al., 2005; Sutton et al., 2005).

It was decided that the best way to compare the results from models having different resolutions is to calculate the mean density on the surface of a sphere at a given altitude. The mean values are obtained by first taking the density value in each grid cell and multiplying it by the area of that cell, and then summing these products. In the case of the HASDM database, the interpolated values are used. As the grid areas were precomputed in units of square radians, the integrated totals only need to be divided by 4π to obtain the mean value in units of kg/m³. In the example in Figure 3, the means are indicated above each map in the upper-right corners. These values were computed for every 3 hr interval in the SET HASDM density database, for the entire 20-year time period, at altitudes of 200, 300, 400, 600, and 800 km. The results are shown as a function of time in Figure 4, with the HASDM values indicated with the black lines and the EXTEMPLAR results drawn with the red lines. For comparison, density values from the NRLMSIS 2.0 model, without the exospheric temperature modifications, are shown with the blue lines to show whether or not the EXTEMPLAR model yields improvements. The red lines are more visible as they are drawn last. Solar wind velocity and IMF values measured by the Advanced Composition Explorer (ACE) spacecraft during this time period were input to the Poynting flux model used in the EXTEMPLAR program, using the Level 2 science data.

Obviously, the three models are in excellent agreement at most altitudes, although HASDM often has slightly larger values. The differences are largest at 200 km. While the models track the same trends over time, the HASDM values at this altitude tend to be larger than from EXTEMPLAR and NRLMSIS. However, as illustrated in Figure 2, at 200 km altitude the variations in the exospheric temperature have little influence on the density at this altitude; the density values at this altitude are determined almost entirely by the conditions calculated within the NRLMSIS 2.0 model. One thing apparent in Figure 4 is that the density changes at 600–800 km span a range of over two decades, while at 200 km the range is only a factor of five. Additional details can be seen in Supporting Information S1 document that contains 20 separate plots for each of the years in the SET HASDM density database. This supplement contains an additional 20 plots with the logarithm of the ratios of the EXTEMPLAR and NRLMSIS densities with respect to the HASDM densities.

A closer look at the time period spanning years 2001 through 2004 is shown in Figure 5, for altitudes 800, 600, 400, and 300 km, from top to bottom. The periodic geomagnetic activity due to the solar rotation and major storms are more visible in this graph. Departures between the EXTEMPLAR and NRLMSIS results are more apparent.

An expanded look at the active time period in late 2003 is presented in Figure 6, covering the time period from 16 October through 24 November 2003, containing two extreme geomagnetic storms. In this graph it is seen that the EXTEMPLAR model (red) tracks the HASDM values (black) better than the NRLMSIS values (blue), and matches the variations during the major storms very well.
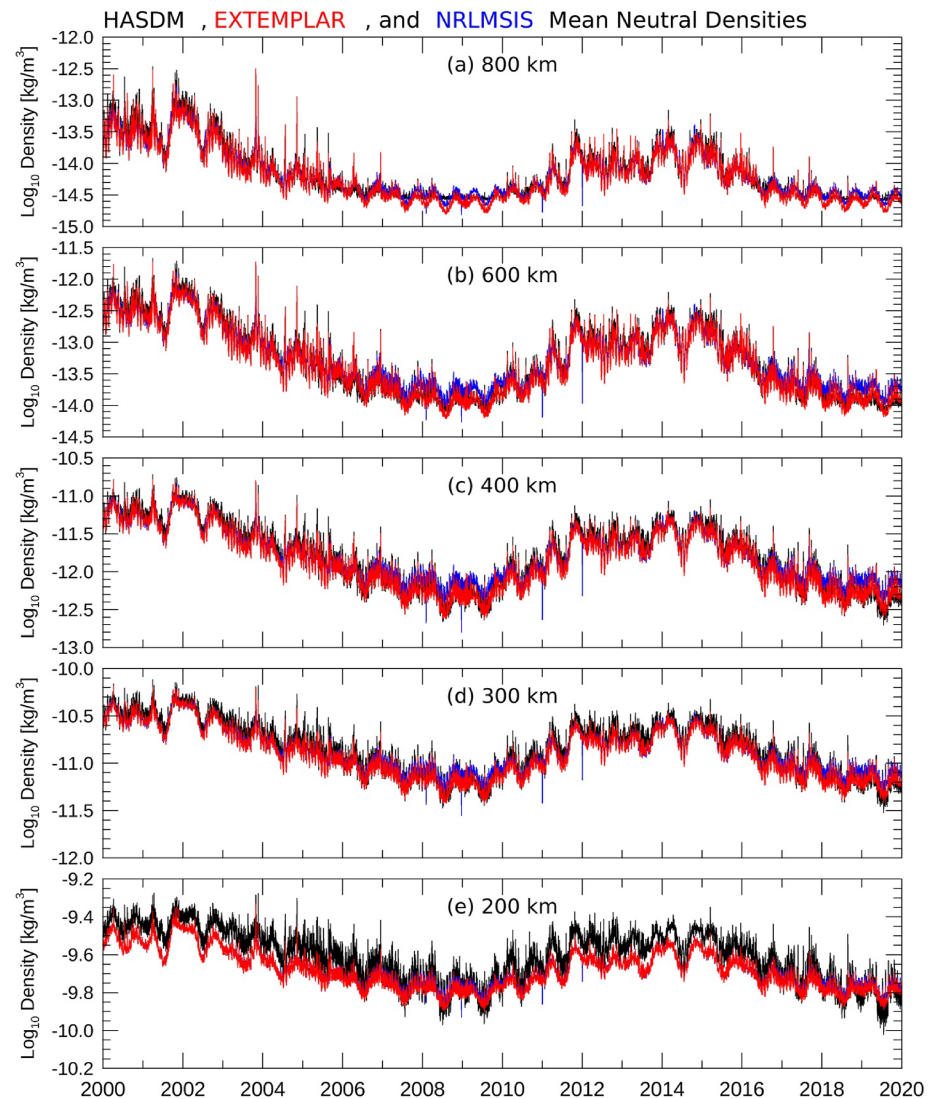
Figure 4. Mean values of densities graphed as a function of time, using a logarithmic scale, for the time period from 1 January 2000 through 31 December 2019. HASDM results are shown in black, EXTEMPLAR in red, and NRLMSIS 2.0 values in blue, for altitudes of 800, 600, 400, 300, and 200 km (top to bottom).

Figure 7 contains another interesting time period, from 1 July 2004 through 30 November 2004. The first event within this interval has three, successive peaks in the neutral density, followed by an event in November having two larger density peaks in succession. In both events the EXTEMPLAR results track the HASDM results very well, particularly in the rapid decline in the densities after the peaks, although there are time periods where the unmodified NRLMSIS model does better in matching the HASDM variations.

5. Correlations, Standard Deviations, and Ratios

Linear correlation coefficients of the mean density values were calculated for each of the 20 years, with the results shown in Figure 8. Figure 8a shows the correlations between the EXTEMPLAR and HASDM values, while Figure 8e to the right shows the NRLMSIS-HASDM correlations. The blue, red, green, brown, and black lines represent altitudes of 200, 300, 400, 600, and 800 km, respectively. In general, the EXTEMPLAR-HASDM correlations range from 0.90 to 0.98 for altitudes of 300–600 km, while the correlation for 200 km altitude tends to range from only 0.82 to 0.94. The correlations at 800 km are more variable, being in the high range in some years, but decreasing in years associated with low solar activity (2007–2009 and 2018–2019). The NRLMSIS
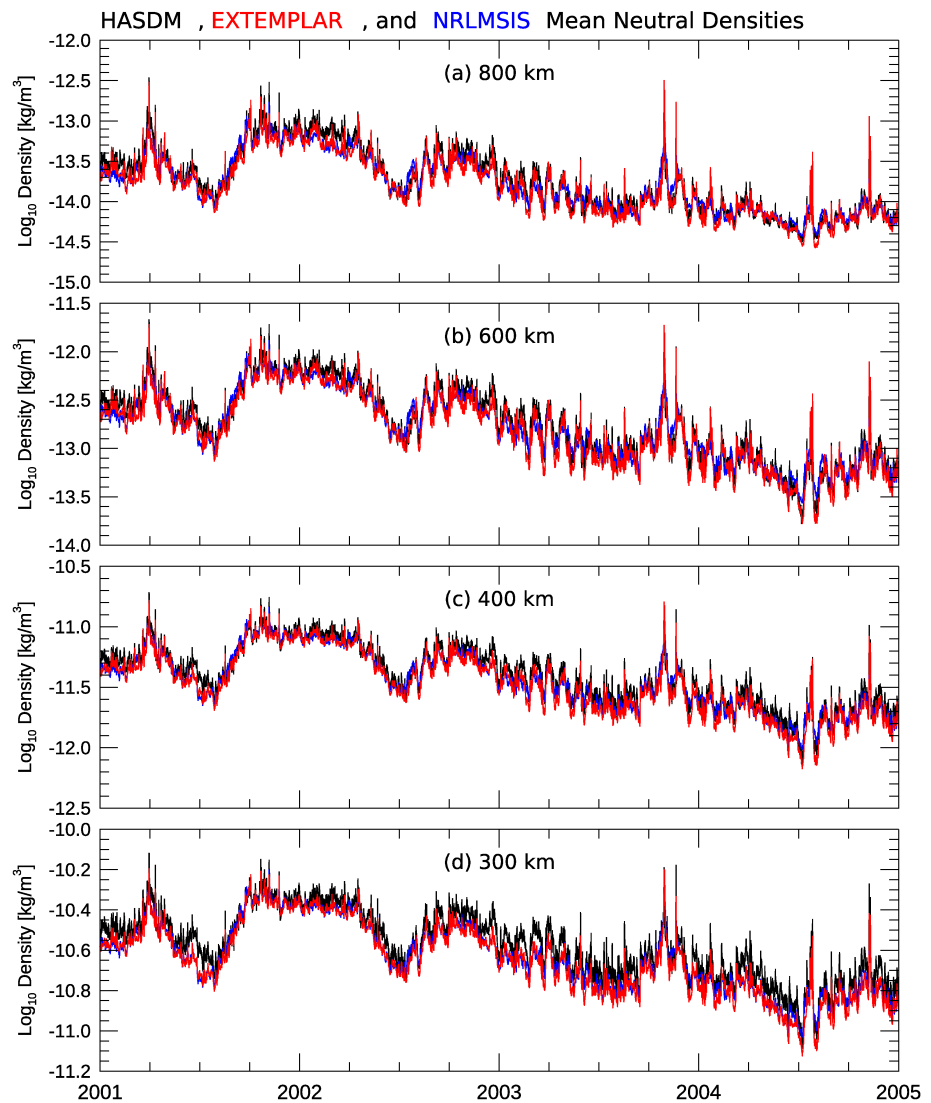
Figure 5. Mean values of densities graphed as a function of time, using a logarithmic scale, for the time period from 1 January 2001 through 31 December 2004. HASDM results are shown in black, EXTEMPLAR in red, and NRLMSIS 2.0 values in blue, for altitudes of 800, 600, 400, and 300 km (top to bottom).

model has correlations with HASDM that are generally lower, with differences ranging from about 0.02 to 0.1, and greater differences (worse correlation) at 800 km altitude.

Standard deviations are shown in Figure 8b for EXTEMPLAR and Figure 8f for NRLMSIS, using the same line coloring at each altitude. Dividing these deviations by the mean of the HASDM density in each year results in the deviation expressed as a percentage, shown in Figures 8c and 8g. With the exception of the deviations at 800 km altitude before 2005, these percentage errors mostly fall in the range of 10%–20% for EXTEMPLAR. The standard deviations for NRLMSIS are approximately the same at altitudes of 200–400 km, except much higher (worse) at 400 km during the times of low solar activity. At 600 and 800 km altitudes the NRLMSIS standard deviations tend to be always greater than the EXTEMPLAR values.

The bottom row in Figure 8 shows the ratios between the model densities as a function of time. Figure 8d shows the base 10 logarithm of EXTEMPLAR/HASDM density ratios and Figure 8h to the right shows the same for NRLMSIS/HASDM ratios. Ideally, the ratio should be one, with a logarithm of zero. Most of the time the logarithm of the EXTEMPLAR ratios in Figure 8d are in the range of about −0.1 to −0.05 (indicating densities slightly less than the HASDM values by a factor of 0.79–0.89), with better results at 600 and 800 km in the years
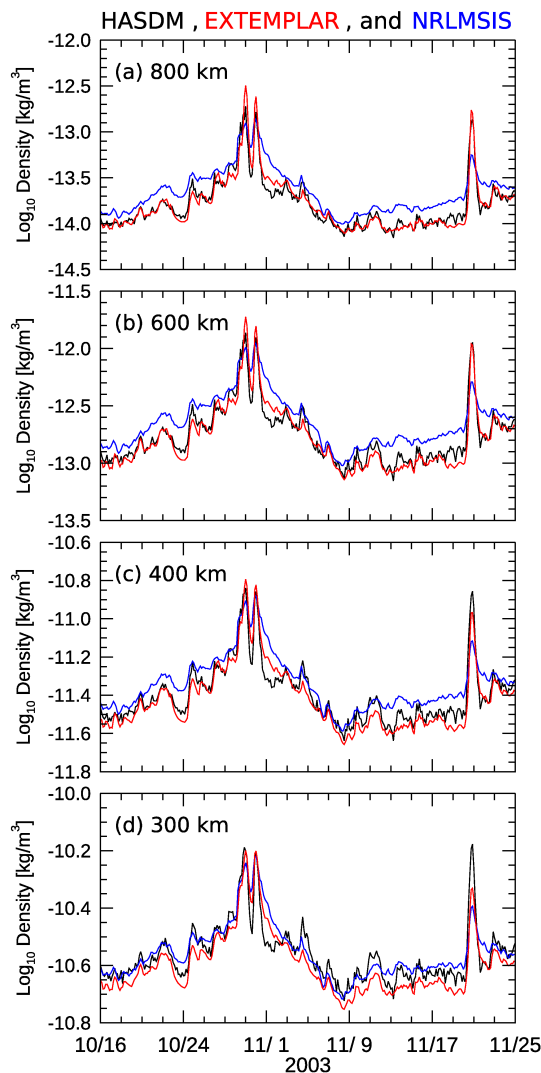
Figure 6. Mean values of densities graphed as a function of time, using a logarithmic scale, for the time period from 16 October through 24 November 2003. HASDM results are shown in black, EXTEMPLAR in red, and NRLMSIS 2.0 values in blue, for altitudes of 800, 600, 400, and 300 km (top to bottom).

2006, 2007, and 2019. The NRLMSIS ratios had greater variability over time and at different altitudes, ranging from negative to positive ratios, particularly during the years of low solar activity (2007–2009 and 2018–2019).

For comparison with our results, Figure 9 contains estimates of the HASDM errors, that were produced by B. Bowman and provided by Tobiska et al. (2021) in a supplement at https://spacewx.com/hasdm/. These errors are derived within HASDM by a process known as the Dynamic Calibration Atmosphere (DCA) (Storz et al., 2005). The dots in Figure 8 show the HASDM error as a percentage, for each of the calibration satellites. The HASDM errors tend to range between 2% and 6% during the peaks in the solar cycle (e.g., Figures 8a and 8c) and increasing to 4%–10% when solar activity is low (e.g., Figures 8b and 8d). These uncertainties were obtained by comparing the derived HASDM data assimilated densities with sets of densities derived from segmented tracking orbit fits to calibration satellites. It is seen in these graphs that the errors are largest at 750 km altitude and above.

6. Discussion

The method in which the neutral densities from different models were integrated over the surface of a sphere at a given altitude has proven to be an effective way to make comparisons. The results show a very good agreement between the EXTEMPLAR and HASDM models on scales ranging from years down to hours. The correlations between the two models at the smallest scales, as seen in Figures 6 and 7 are excellent. The EXTEMPLAR predictions match the HASDM values especially well during the most extreme events, most notably at 400 km altitude and above. In general, the EXTEMPLAR method improved upon the unmodified density predictions from the NRLMSIS model, resulting in higher correlations, lower standard deviations, and more consistent ratios in comparison with the HASDM densities. However, there are times when the NRLMSIS model is in better agreement with the HASDM values.

The results shown here are helpful for illustrating how the thermosphere behaves over time at different altitudes, including the annual and solar cycle variability in addition to during major events. It is seen that geomagnetic storms have the greatest influence at higher altitudes, where there are substantial changes in the neutral density with respect to pre-storm levels.

The correlations graphed in Figure 8a for the EXTEMPLAR-HASDM densities at altitudes of 300–600 km are approximately 0.95, which we consider to be very good. While the correlations a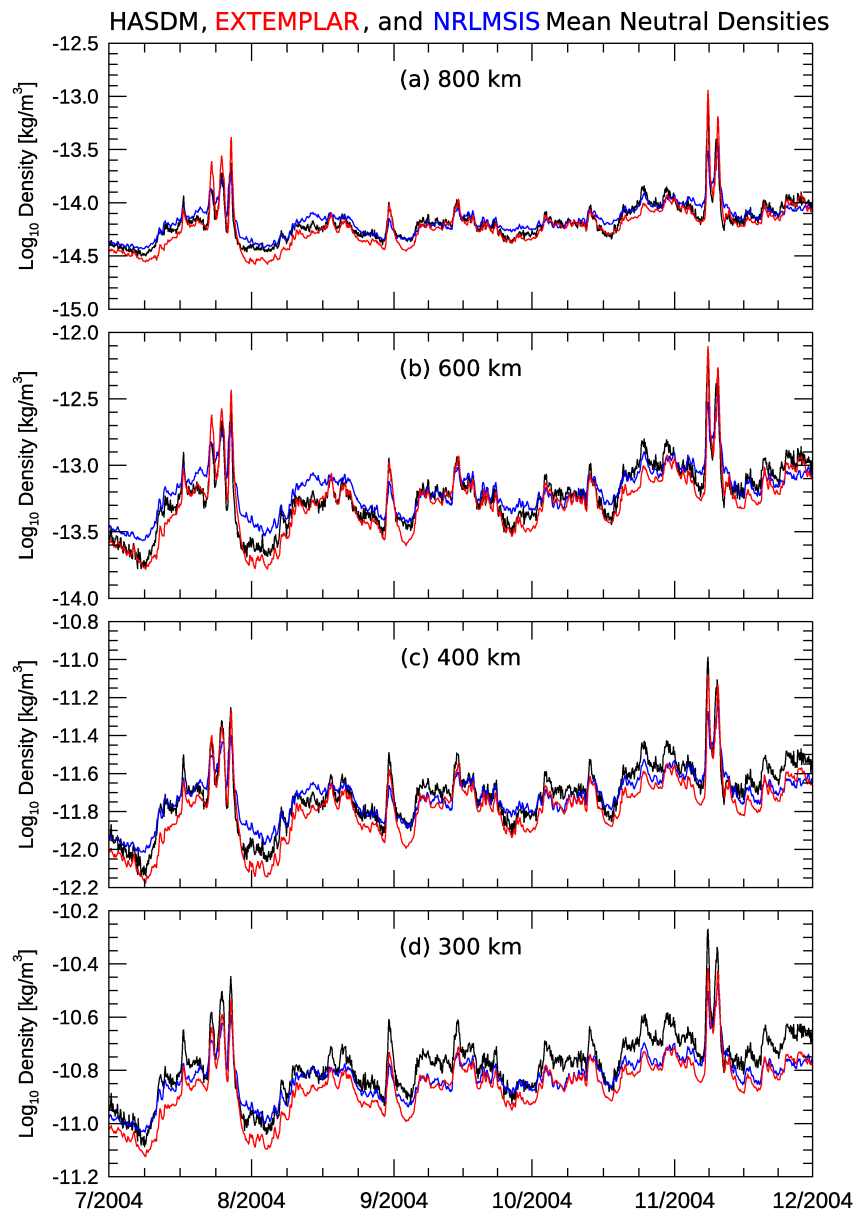t 200 km altitude are lower (in the range of 0.82–0.94), they are still reasonable. At 200 km altitude the exospheric temperature calculations have little effect on the density variations, as shown in Figure 2.

Results at 800 km are the most inconsistent. Figure 9 also indicates that the HASDM errors are the largest here, particularly during times of low solar activity, as shown in Figures 9b and 9d. Solar minimum also coincides with the lowest correlations at 800 km (black line in Figure 8). The plots in Supporting Information S1 for the years 2007–2009, and 2017–2019 show that the densities from the HASDM system have a relatively flat line at this altitude, while the NRLMSIS model produced variations in the density that are the expected signatures of the semi-annual oscillations (Emmert & Picone, 2010). As the EXTEMPLAR method uses NRLMSIS to calculate densities, it also has the semi-annual oscillations. The most likely explanation for the flat response in the HASDM system is that the model it is based on lacks sufficient variation in the amount of atomic oxygen and or helium.

At 800 km altitude the EXTEMPLAR densities tend to exceed the HASDM values during the large geomagnetic storms, such as in late October in Figure 6a. This is the cause of the increase in the black line in 2003 in Figure 8c.

Figure 7. Mean values of densities graphed as a function of time, using a logarithmic scale, for the time period from 1 July 2004 through 30 November 2004. HASDM results are shown in black, EXTEMPLAR in red, and NRLMSIS 2.0 values in blue, for altitudes of 800, 600, 400, and 300 km (top to bottom).

It can be argued that the densities calculated by the EXTEMPLAR-MSIS combination could more accurate than HASDM at this altitude, since the sparse atmosphere may have little effect on the segmented orbit density fits.

It was mentioned earlier that HASDM has a coarse spatial resolution, while satellite measurements indicate that the density often varies over distances that are smaller than can be resolved with this model. In cases were the total densities of the two models are in agreement, the EXTEMPLAR-MSIS combination is likely more accurate.

Oftentimes the integrated densities from HASDM are slightly greater than those from EXTEMPLAR. In a comparison between the SET HASDM data set with the JB2008 model and CHAMP and GRACE density measurements, Licata et al. (2021) had found that the HASDM density values were also consistently greater than the values derived from the CHAMP and GRACE accelerometer measurements, while matching better than the JB2008 model. Licata et al. (2021) also found that during the major storm in October 2003 (the same event shown here in
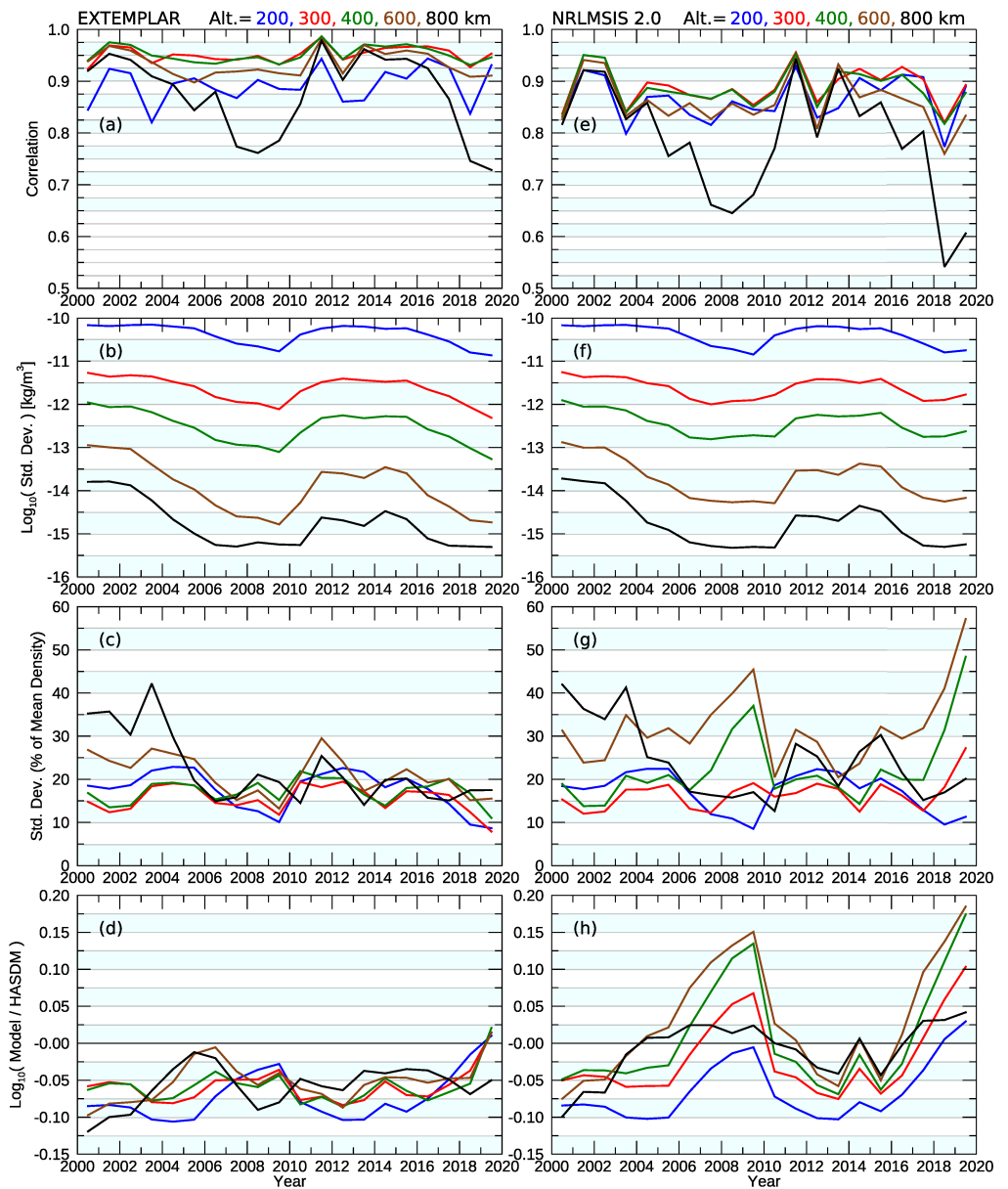
Figure 8. Model correlations, standard deviations, and ratios. EXTEMPLAR results are in the left column and NRLSIS 2.0 results are in the right column. (a and e) Coefficients of correlation for all years. The blue, red, green, brown, and black lines represent altitudes of 200, 300, 400, 600, and 800 km, respectively. (b and f) Standard deviations, in units of kg/m^3, using the same line colors. (c and (g Standard deviations expressed as a percentage of the HASDM mean density in each year. (d and h) Base 10 logarithm of the ratio between the model and HASDM density, showing the mean value in each year.

the first half of Figure 6), while the HASDM data set had slightly larger densities than measured with CHAMP and GRACE, it did very well at matching the relative changes in density during this period.

It would be possible to modify the NRLMSIS model to bring it (and EXTEMPLAR) in better agreement with the HASDM densities. For example, changes could be made in composition and derivatives at the lower boundary of the thermosphere. On the other hand the density values from HASDM may have a bias, so first it would be necessary to resolve the reasons for why the HASDM and NRLMSIS models differ at some altitudes before committing to any modifications. As reported by Emmert (2015), the estimation of coefficients of drag and ballistic coefficients "is quite challenging even for objects whose mass, geometry, and composition are precisely known."
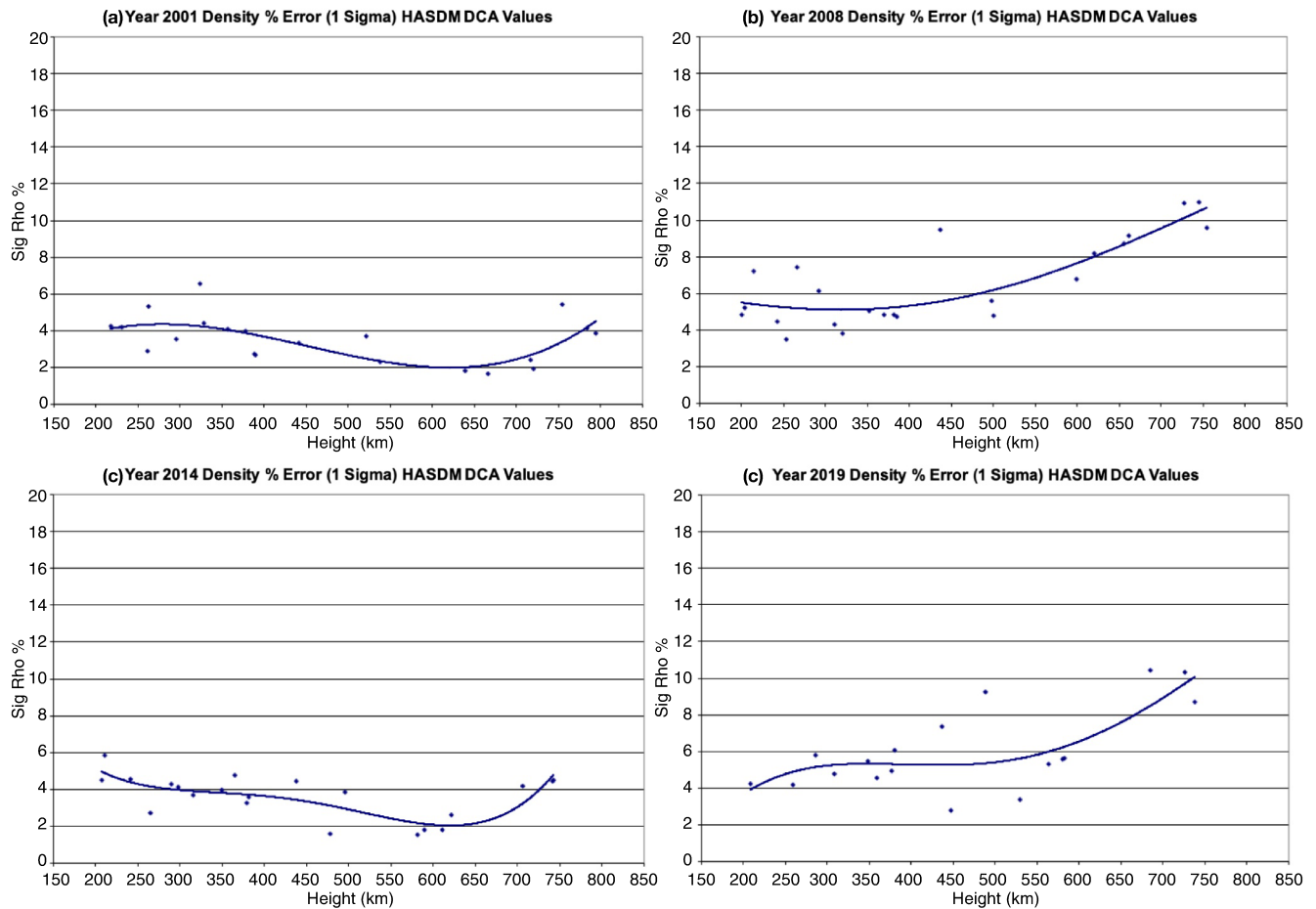
Figure 9. HASDM errors as a function of altitude. The four parts show the errors for the years (a) 2001, (b) 2008, (c) 2014, and (d) 2019.

7. Conclusion

The comparison of the densities calculated by the EXTEMPLAR program with the values in the SET HASDM density database show that EXTEMPLAR performs very well. As the HASDM assimilation system relies on radar tracking of multiple satellites to derive the neutral densities, it is expected to be very accurate. But it cannot predict the response of the neutral density to sudden geomagnetic storms in advance, before the tracking measurements can be obtained. On the other hand, the EXTEMPLAR program can use the real-time measurements of the solar wind velocity and IMF to make predictions approximately 1 hr ahead of the thermosphere's response to extreme space weather events. This lead provides time to issue alerts or calculate perturbations to satellite orbits.

The EXTEMPLAR results shown here had used Level 2 science data from the ACE satellite, which had a better quality than the real-time data provided by ACE. Presently the real-time solar wind measurements are provided by the Deep Space Climate Observatory (DSCOVR). The quality of the real-time DSCOVR solar wind and magnetic field measurements are just as good as the ACE Level 2 data, so this change will not degrade the performance of EXTEMPLAR. The solar indices are also updated in near real time by SET.

Other developers of thermosphere models, either empirical or numerical, are encouraged to compare their neutral density calculations with the SET HASDM density database in a similar manner. The total, integrated densities shown in Figure 4 are available in an archive at https://doi.org/10.5281/zenodo.5177065 for the entire, 20 year time period. As mentioned earlier, these data are of value for studying how the neutral density at different altitudes vary on time scales ranging from hours to solar cycles.

Data Availability Statement

A data archive containing the mean neutral densities on spherical shells at altitudes of 200, 300, 400, 600, and 800 km, from both EXTEMPLAR and HASDM, is available at https://doi.org/10.5281/zenodo.5177065. Supporting Information S1 contains graphs of these mean densities for each of the 20 years. The original SET HASDM database access and supplementary information can be found at https://spacewx.com/hasdm/. The ACE level 2 data are available from the NASA archives at https://cdaweb.gsfc.nasa.gov/pub/data/ace. The solar indices are available at https://spacewx.com/jb2008/.

References

Astafyeva, E., Zakharenkova, I., Huba, J. D., Doornbos, E., & van den IJssel, J. (2017). Global ionospheric and thermospheric effects of the June 2015 geomagnetic disturbances: Multi-instrumental observations and modeling. *Journal of Geophysical Research: Space Physics*, *112*, 11716–11742. https://doi.org/10.1002/2017JA024174

Bowman, B. R., Tobiska, W. K., Marcos, F. A., Huang, C. Y., Lin, C. S., & Burke, W. J. (2008). A new empirical thermospheric density model JB2008 using new solar and geomagnetic indices. In *AIAA/AAS Astrodynamics Specialist Conference Proceedings*. https://doi.org/10.2514/6.2008-6438

Bruinsma, S., Forbes, J. M., Nerem, R. S., & Zhang, X. (2006). Thermosphere density response to the 20–21 November 2003 solar and geomagnetic storm from CHAMP and GRACE accelerometer data. *Journal of Geophysical Research*, *111*. https://doi.org/10.1029/2005JA011284

Bruinsma, S., Sutton, E., Solomon, S. C., Fuller-Rowell, T., & Fedrizzi, M. (2018). Space weather modeling capabilities assessment: Neutral density for orbit determination at low earth orbit. *Space Weather*, *16*(11), 1806–1816. https://doi.org/10.1029/2018SW002027

Bruinsma, S., Tamagnan, D., & Biancale, R. (2004). Atmospheric densities derived from CHAMP/STAR accelerometer observations. *Planetary and Space Science*, *52*, 297–312. https://doi.org/10.1016/j.pss.2003.11.004

Case, N. A., & Wild, J. A. (2012). A statistical comparison of solar wind propagation delays derived from multispacecraft techniques. *Journal of Geophysical Research: Space Physics*, *117*(A2). https://doi.org/10.1029/2011JA016946

Crowley, G., Knipp, D. J., Drake, K. A., Lei, J., Sutton, E., & Lühr, H. (2010). Thermospheric density enhancements in the dayside cusp region during strong B_y conditions. *Geophysical Research Letters*, *37*. https://doi.org/10.1029/2009GL042143

Emmert, J. T. (2015). Thermospheric mass density: A review. *Advances in Space Research*, *56*(5), 773–824. https://doi.org/10.1016/j.asr.2015.05.038

Emmert, J. T., Drob, D. P., Picone, J. M., Siskind, D. E., Jones, M., Jr., Mlynczak, M. G., et al. (2020). NRLMSIS 2.0: A whole-atmosphere empirical model of temperature and neutral species densities. *Earth and Space Science*, *7*, e2020EA001321. https://doi.org/10.1029/2020EA001321

Emmert, J. T., & Picone, J. M. (2010). Climatology of globally averaged thermospheric mass density. *Journal of Geophysical Research*, *115*(A9). https://doi.org/10.1029/2010JA015298

Friis-Christensen, E., Lühr, H., & Hulot, G. (2006). Swarm: A constellation to study the Earth's magnetic field. *Earth, Planets and Space*, *58*(4), 351–358. https://doi.org/10.1186/BF03351933

Hedin, A. E. (1991). Extension of the MSIS thermosphere model into the middle and lower atmosphere. *Journal of Geophysical Research*, *96*, 1159–1172. https://doi.org/10.1029/90ja02125

Licata, R. J., Mehta, P. M., Tobiska, W. K., Bowman, B. R., & Pilinski, M. D. (2021). Qualitative and quantitative assessment of the SET HASDM database. *Space Weather*, *19*(8), e2021SW002798. https://doi.org/10.1029/2021SW002798

Mehta, P. M., Walker, A. C., Sutton, E. K., & Godinez, H. C. (2017). New density estimates derived using accelerometers on board the CHAMP and GRACE satellites. *Space Weather*, *15*(4), 558–576. https://doi.org/10.1002/2016SW001562

Picone, J., Hedin, A., Drob, D., & Aikin, A. (2002). NRLMSISE-00 empirical model of the atmosphere: Statistical comparisons and scientific issues. *Journal of Geophysical Research*, *107*(A12). https://doi.org/10.1029/2002JA009430

Prölss, G. W., & Bird, M. K. (2004). *Physics of the Earth's space environment: An introduction*. Springer-Verlag Berlin Heidelberg. https://link.springer.com/book/10.1007/978-3-642-97123-5

Reigber, C. H., Lühr, H., & Schwintzer, P. (2002). CHAMP mission status. *Advances in Space Research*, *30*(2), 129–134. https://doi.org/10.1016/S0273-1177(02)00276-4

Schlegel, K., Lühr, H., St.-Maurice, J.-P., Crowley, G., & Hackert, C. (2005). Thermospheric density structures over the polar regions observed with CHAMP. *Annales Geophysicae*, *23*, 1659–1672. https://doi.org/10.5194/angeo-23-1659-2005

Storz, M. F., Bowman, B. R., Branson, M. J. I., Casali, J. S., & Tobiska, W. K. (2005). High accuracy satellite drag model (HASDM). *Advances in Space Research*, *36*(12), 2497–2505. https://doi.org/10.1016/j.asr.2004.02.020

Sutton, E. K. (2008). *Effects of solar disturbances on the thermosphere densities and winds from CHAMP and GRACE satellite accelerometer data* (Unpublished doctoral dissertation). University of Colorado.

Sutton, E. K., Forbes, J. M., & Nerem, R. S. (2005). Global thermospheric neutral density and wind response to the severe 2003 geomagnetic storms from CHAMP accelerometer data. *Journal of Geophysical Research*, *110*. https://doi.org/10.1029/2004JA010985

Tapley, B. D., Watkins, S. B. M., & Reigber, C. (2004). The gravity recovery and climate experiment: Mission overview and early results. *Geophysical Research Letters*, *31*. https://doi.org/10.1029/2004gl019920

Thayer, J. P., Tobiska, W. K., Pilinski, M. D., & Sutton, E. K. (2021). Remaining issues in upper atmosphere satellite drag. In *Space weather effects and applications* (pp. 111–140). American Geophysical Union (AGU). https://doi.org/10.1002/9781119815570.ch5

Tobiska, W. K., Bouwer, S. D., & Bowman, B. R. (2008). The development of new solar indices for use in thermospheric density modeling. *Journal of Atmospheric and Solar-Terrestrial Physics*, *70*, 803–819. https://doi.org/10.1016/j.jastp.2007.11.001

Tobiska, W. K., Bowman, B. R., Bouwer, S. D., Cruz, A., Wahl, K., Pilinski, M. D., et al. (2021). The SET HASDM density database. *Space Weather*, *19*(4), e2020SW002682. https://doi.org/10.1029/2020SW002682

van den IJssel, J., Doornbos, E., Iorfida, E., March, G., Siemes, C., & Montenbruck, O. (2020). Thermosphere densities derived from Swarm GPS observations. *Advances in Space Research*, *65*(7), 1758–1771. https://doi.org/10.1016/j.asr.2020.01.004

Weimer, D. R. (2005a). Improved ionospheric electrodynamic models and application to calculating Joule heating rates. *Journal of Geophysical Research*, *110*(A5). https://doi.org/10.1029/2004JA010884

Weimer, D. R. (2005b). Predicting surface geomagnetic variations using ionospheric electrodynamic models. *Journal of Geophysical Research*, *110*(A12). https://doi.org/10.1029/2005JA011270

Weimer, D. R., Mehta, P. M., Tobiska, W. K., Doornbos, E., Mlynczak, M. G., Drob, D. P., & Emmert, J. T. (2020). Improving neutral density predictions using exospheric temperatures calculated on a geodesic, polyhedral grid. *Space Weather*, *18*(1), e2019SW002355. https://doi.org/10.1029/2019SW002355

Weimer, D. R., Mlynczak, M. G., Emmert, J. T., Doornbos, E., Sutton, E. K., & Hunt, L. A. (2018). Correlations between the thermosphere's semiannual density variations and infrared emissions measured with the SABER instrument. *Journal of Geophysical Research: Space Physics*, *123*, 8850–8864. https://doi.org/10.1029/2018JA025668

Weimer, D. R., Sutton, E. K., Mlynczak, M. G., & Hunt, L. A. (2016). Intercalibration of neutral density measurements for mapping the thermosphere. *Journal of Geophysical Research*, *121*, 5975–5990. https://doi.org/10.1002/2016JA022691